Mathematical Biosciences and Engineering

https://www.aimspress.com/journal/mbe

MBE, 23(7): 1995–2017.
DOI: 10.3934/mbe.2026073
Received: 02 April 2026
Revised: 27 May 2026
Accepted: 02 June 2026
Published: 08 July 2026

Research article

Modeling transmission intensity in SI epidemics via CIR and Jacobi processes: Asymptotic results and preliminary intervention strategies

León A. Valencia*, Raúl Alejandro Morán-Vásquez and Duván H. Cataño Salazar

Instituto de Matemáticas, Universidad de Antioquia, Calle 67 No. 53-108, Medellín 050010, Colombia

* **Correspondence:** Email: lalexander.valencia@udea.edu.co; Tel: +573117996116.

Abstract: This paper studies an SI epidemic model with stochastic transmission rates of the form $(\beta_t = \varphi(t)P_t : t \geq 0)$, where $\varphi(t)$ is a deterministic modulation function and P_t is a positive stochastic process. We show that the asymptotic behavior of the epidemic is determined by the integrated intensity process $(H_t = \int_0^t \beta_s\, ds : t \geq 0)$. We consider two stochastic models for $(P_t : t \geq 0)$: the bounded Jacobi process and the Cox–Ingersoll–Ross (CIR) process. Both preserve positivity, but differ in the support of their sample paths. In the non-modulated regime ($\varphi \equiv 1$), the CIR framework allows explicit expressions for Laplace transforms and probabilistic bounds associated with the integrated intensity process. Additionally, we present numerical simulations in two regimes: the non-modulated case ($\varphi(t) = 1$) and the exponentially damped case ($\varphi(t) = e^{-\alpha t}$). The simulations show that the bounded and unbounded structures of the stochastic transmission processes produce different tail behaviors, particularly in high-volatility regimes.

Keywords: Cox–Ingersoll–Ross process; Jacobi process; random transmission rates; SDEs; stochastic epidemiological models

1. Introduction

The quantitative study of infectious diseases fundamentally relies on describing how susceptible and infected individuals meet and interact. The first study of this type of phenomenon is generally attributed to [1]. In that work, it was proposed that the rate of new infections is proportional to the product of the densities of both groups. This assumption still remains in many modern epidemiological models. The conceptual approach introduced in [2] was formalized with greater mathematical rigor in [3]. Deterministic modeling continues to serve as a reference to understand this phenomenon [4–6].

Below we provide a brief description of the model. Consider a population of N individuals divided into two groups, susceptible (S) and infected (I), whose infection dynamics follow the deterministic

system

$$\begin{cases} \dfrac{dS(t)}{dt} = -\beta \dfrac{S(t)I(t)}{N}, \\ \dfrac{dI(t)}{dt} = \beta \dfrac{S(t)I(t)}{N}, \end{cases}$$

for $t \geq 0$, where $\beta > 0$ represents the transmission rate and the total population satisfies $S(t) + I(t) = N$. Here, β is traditionally interpreted as the product of the average number of contacts per unit time and the probability of transmission per contact.

To simplify the analysis, we introduce the normalized variables

$$S_t = \frac{S(t)}{N}, \qquad I_t = \frac{I(t)}{N},$$

which represent the proportions of susceptible and infected individuals, respectively. Since the total population remains constant, we have $S_t + I_t = 1$.

In terms of these normalized variables, and observing that $I_t = 1 - S_t$, the system reduces to the following ordinary differential equation:

$$\frac{dS_t}{dt} = -\beta S_t(1 - S_t), \qquad S_0 = s_0 \in (0, 1). \tag{1.1}$$

While Eq (1.1) describes a purely deterministic evolution, transmission rates are naturally subject to temporal variability. More specifically, this variability may arise from time-dependent changes in contact patterns due to social behavior or mobility, as well as fluctuations in effective infectivity driven by environmental conditions or population heterogeneity. To capture this uncertainty, we transition to a stochastic framework by replacing the constant parameter β with a stochastic process $(\beta_t : t \geq 0)$, thus leading to the stochastic differential equation (SDE) studied in this work. This approach differs from classical additive-noise formulations, where randomness is introduced as a perturbation of a constant transmission rate, and instead models the transmission rate itself as an intrinsically positive stochastic process.

The literature offers several methods to incorporate the randomness that naturally occurs in these systems. For instance, [7] investigated the effects of treating the initial condition as a random variable rather than a fixed value. While that study analyzed the random time required to reach a specific infection threshold, randomizing the initial state does not alter the system's asymptotic behavior, thereby entailing that the entire population becomes infected. This suggests that to model phenomena where a significant portion of the population remains susceptible, randomness must be incorporated into the evolution of the process, rather than solely in its initialization.

More recent approaches have considered stochastic perturbations which act directly on the transmission dynamics, including stochastic transmission coefficients, mean-reverting transmission mechanisms, and epidemic models that evolve under environmental noise [8–10]. In particular, the work of Albani and Zubelli [9] models the transmission coefficient itself as a stochastic process with temporal variability, which is a perspective closely related to the framework considered in the present paper. Related stochastic epidemic frameworks based on Cox-Ingersoll-Ross (CIR)-type dynamics and empirical calibration were studied in [11], while hybrid approaches that combined stochastic epidemic dynamics with agent-based or data-driven methodologies were considered in [12]. Moreover, structural

heterogeneity and healthcare-system variability in epidemic outcomes were analyzed in [13]. These formulations incorporate temporal variability and heterogeneous epidemic effects beyond deterministic models.

In contrast, the present work focuses on the analytical and asymptotic properties of stochastic transmission dynamics within a stylized SI framework.

A common approach consists in transforming the deterministic equation (1.1) into an SDE of the following form:

$$dS_t = \mu(S_t)dt + G(S_t)dW_t, \qquad S_0 = s_0 \in (0,1), \tag{1.2}$$

where W_t is a standard Wiener process defined on a complete filtered probability space $(\Omega, \mathcal{F}, \{\mathcal{F}_t\}_{t\geq 0}, \mathbb{P})$. The drift coefficient $\mu(\cdot)$ and the diffusion coefficient $G(\cdot)$ characterize the deterministic trend and the intensity of the stochastic fluctuations, respectively. Typically, noise is introduced through the following perturbation:

$$\beta_t dt = \beta dt + \sigma dW_t,$$

where $\sigma > 0$ measures the intensity of the white noise. In contrast, in our framework, the transmission rate is modeled as follows:

$$\beta_t = \varphi(t)P_t,$$

where P_t is the strong solution of an SDE, and $\varphi(t)$ is a deterministic modulation. In general, this representation does not lead to an additive-noise SDE for β_t, except in the special case where $\varphi(t)$ is constant.

The mathematical regularity of this standard framework is well established. In particular, by employing Lyapunov functions, it is possible to show that trajectories remain within the interval $(0, 1)$ almost surely [14]. Furthermore, if the noise intensity is sufficiently small, then the stochastic process $(S_t)_{t\geq 0}$ possesses a unique limiting distribution with support on $(0, 1)$, thus preventing the total extinction of the susceptible population.

In this paper, we explore a modeling approach that differs from those traditionally studied in the mathematical literature. Instead of perturbing the transmission rate with additive noise, we model the infection rate itself as a stochastic process that is positive by construction. Specifically, we consider the CIR process and a Jacobi-type diffusion on $[0, a]$ to modulate the transmission dynamics. While these processes preserve positivity and possess well-known mathematical properties, they share a common asymptotic drawback: without further intervention, the population eventually tends toward a fully infected state.

This motivates the introduction of a time-dependent modulation within the stochastic framework. Formally, we define the transmission rate as follows:

$$\beta_t = \varphi(t)P_t,$$

where P_t represents the intrinsic stochasticity of the infection process, and $\varphi(t)$ is a deterministic modulation function. This multiplicative structure allows the modulation function to scale the transmission intensity and its variability, thereby reflecting that a reduction in the average contact rate also reduces the absolute variability of the infection process. From a modeling perspective, this deterministic modulation may also be interpreted as a simplified representation of aggregate changes in the transmission

intensity associated with intervention effects or behavioral changes over time. Under suitable integrability conditions on φ, we show that this modulation function can alter the asymptotic regime, thus allowing the cumulative transmission intensity to remain finite.

We note that the intervention function is modeled here as a deterministic input in order to isolate its effect on the transmission dynamics. More general formulations, where the modulation function depends on the state of the epidemic or incorporates feedback mechanisms, constitute a natural extension of the present framework. Another interesting direction for future research is the estimation of the modulation function $\varphi(t)$ from epidemic data by comparing transmission dynamics before and after the implementation of control measures.

We emphasize that the present framework is intended as a stylized model aimed at isolating the role of stochastic transmission dynamics. While the SI structure does not account for recovery or immunity, it provides a tractable setting to analyze how variability in the transmission rate influences the epidemic evolution. Extensions to more complex compartmental models, such as SIR-type dynamics, constitute a natural direction for future research. In this context, the present work primarily focuses on the analytical properties of the model, while empirical calibration and validation are left for future investigation.

The remainder of the article is organized as follows. Section 2 establishes the general stochastic framework for the SI model and provides proofs that describe the system behavior under different intervention scenarios. Sections 2.1 and 2.2 introduce the two candidates for the stochastic intensity: the bounded Jacobi process and the unbounded CIR process. In Section 2.3, we analyze the random time required to reach critical thresholds within the CIR framework under a non-intervention regime, thereby deriving an analytical risk monitor based on Chernoff bounds. Finally, Section 4 provides a numerical comparison which illustrates how the choice of stochastic driver affects the estimation of extreme risks, followed by concluding remarks in Section 5.

2. General model formulation and asymptotic results

To build our framework, we consider an SI model in a population of unit size ($N = 1$), where S_t represents the proportion of individuals still susceptible at time t. Unlike traditional deterministic approaches, we assume the transmission rate is driven by a stochastic process $(\beta_t)_{t\geq 0}$ with continuous and almost surely (a.s.) positive sample paths. Under these assumptions, the epidemic dynamics are described by the following equation:

$$\frac{dS_t}{dt} = -\beta_t S_t(1 - S_t), \qquad S_0 = s_0 \in (0, 1). \tag{2.1}$$

We note that, conditionally on the realization of the stochastic process β_t, the equation for S_t can be interpreted as a random ordinary differential equation (RODE), where randomness enters through the transmission rate rather than through a direct diffusion term.

A key advantage of this formulation is its analytical tractability, thereby enabling an explicit solution to the system for any given noise realization. The following proposition provides the exact epidemic trajectory.

Proposition 2.1. *Let $(\beta_t)_{t\geq 0}$ be a stochastic process with a.s. continuous sample paths. Equation* (2.1)

admits a unique global solution given by the following:

$$S_t = \left[1 + \left(\frac{1}{s_0} - 1\right)\exp\left(\int_0^t \beta_r\, dr\right)\right]^{-1}, \qquad t \geq 0. \tag{2.2}$$

Remark. The solution (2.2) is obtained pathwise using classical methods. This expression indicates that the state of the epidemic is determined by the stochastic process ($H_t = \int_0^t \beta_s\, ds : t \geq 0$), which we will call the cumulative transmission intensity.

In our approach, we decompose the transmission rate as $\beta_t = \varphi(t)P_t$. Here, P_t models the randomness of the transmission rate in the absence of any interventions, while $\varphi(t)$ is a deterministic function that modulates the transmission intensity. This decomposition allows us to analyze the final state of the epidemic ($S_\infty = \lim_{t\to\infty} S_t$) by studying the asymptotic behavior of H_t. Specifically, a portion of the population escapes infection (i.e., $S_\infty > 0$) if and only if H_t remains bounded as $t \to \infty$ almost surely.

The following theorem formalizes the conditions under which the modulation function alters the asymptotic behavior of the system.

Theorem 2.2 (Asymptotic Behavior under Integrable Modulation)**.** *Let $\beta_t = P_t\varphi(t)$, where φ is a modulation function that satisfies*

$$\int_0^\infty \varphi(s)\, ds < \infty,$$

and $(P_t)_{t\geq 0}$ is a stochastic process with a.s. continuous positive paths and bounded mean $\sup_{t\geq 0}\mathbb{E}[P_t] \leq M < \infty$*. Then,*

$$S_\infty \in (0, s_0) \quad a.s.$$

Proof. The non-decreasing nature of H_t ensures that H_∞ is a well-defined random variable (taking values in $[0, \infty]$). To guarantee that S_∞ does not vanish, it is sufficient to show that H_∞ is finite almost surely. By applying Fubini's Theorem to the expected value of H_∞, we obtain the following:

$$\mathbb{E}[H_\infty] = \mathbb{E}\left[\int_0^\infty P_s\varphi(s)\, ds\right] = \int_0^\infty \mathbb{E}[P_s]\varphi(s)\, ds \leq M\int_0^\infty \varphi(s)\, ds < \infty.$$

Since the expectation is finite, it follows that $H_\infty < \infty$ a.s. Consequently, from the explicit solution given in (2.2), the susceptible fraction S_∞ remains strictly positive, and specifically $S_\infty \in (0, s_0)$ due to the positivity of H_∞ and the initial condition.

Conversely, when $\varphi(t) \equiv 1$, the system follows the non-modulated stochastic regime.

Theorem 2.3 (Asymptotic Behavior in the Non-Modulated Regime ($\varphi \equiv 1$))**.** *Suppose $(P_t)_{t\geq 0}$ is an ergodic Markov process with a unique stationary distribution π supported on $(0, \infty)$ and a finite mean $\int_0^\infty x\pi(x)\, dx > 0$. Then, $H_\infty = \infty$ a.s., which implies $S_\infty = 0$ a.s.*

Proof. The result follows from the Ergodic Theorem for Markov processes. Given that $\varphi \equiv 1$, the integrated intensity H_t is simply $\int_0^t P_s\, ds$. The time average satisfies the following:

$$\lim_{t\to\infty}\frac{H_t}{t} = \lim_{t\to\infty}\frac{1}{t}\int_0^t P_s\, ds = \int_0^\infty x\pi(x)\, dx > 0 \quad \text{a.s.}$$

This linear growth implies that $H_t \approx t \cdot K$ for a large t and some constant $K > 0$. Consequently, the integrated intensity diverges ($H_\infty = \infty$) almost surely, which results in the extinction of the susceptible population according to the explicit solution (2.2).

2.1. Model I: A bounded rate via the Jacobi process

First, we consider a scenario where the transmission intensity $(P_t^J)_{t\geq 0}$ is governed by a Jacobi process. This formulation is biologically sound, as it reflects the fact that the transmission rate is inherently bounded due to physical and social constraints on human interactions. In practice, individuals can only sustain a finite number of effective contacts per unit of time, limited by factors such as time availability, spatial constraints, and behavioral patterns. The coupled dynamics are described by the following system of SDEs:

$$\begin{cases} dS_t = -P_t^J \varphi(t) S_t (1 - S_t)\, dt, \\ dP_t^J = \theta(\mu - P_t^J)\, dt + \sigma \sqrt{P_t^J (a - P_t^J)}\, dW_t, \end{cases} \tag{2.3}$$

with initial conditions $S_0 = s_0 \in (0, 1)$ and $P_0^J = p_0 \in (0, a)$. Here, $\theta > 0$ represents the mean-reversion speed, $\mu \in (0, a)$ is the long-term mean, and $\sigma > 0$ denotes the volatility coefficient (see [15]).

The parameter $a > 0$ defines the upper bound of the transmission rate, thereby representing the maximum possible intensity of infection under the specific social and environmental conditions of the population. While the CIR process (discussed below) allows for arbitrarily large spikes in transmission, the Jacobi process restricts P_t^J to the compact interval $[0, a]$. This boundedness is consistent with the fact that the number of effective contacts per unit of time is limited by physical and temporal constraints.

To ensure that the process remains in the interval $(0, a)$ and admits a unique stationary distribution, we assume that the parameters satisfy the following:

$$2\theta\mu \geq \sigma^2 a, \qquad 2\theta(a - \mu) \geq \sigma^2 a.$$

Under these conditions, the process remains in $(0, a)$ almost surely for all $t \geq 0$, and its stationary distribution is a Beta distribution supported on $(0, a)$. Moreover,

$$\mathbb{E}[P_t^J] = \mu + (p_0 - \mu)e^{-\theta t}, \qquad t \geq 0.$$

Following the framework established in Section 2, the asymptotic behavior of the epidemic depends on the convergence of the integrated intensity process H_t^J. The following lemma provides an explicit expression for the expected cumulative pressure, which is used to verify the stability conditions of Theorem 2.2.

Lemma 2.4. *Under the Jacobi framework, the expected Integrated Transmission Intensity at time $t \geq 0$ is given by the following:*

$$\mathbb{E}[H_t^J] = \int_0^t \left[\mu + (p_0 - \mu)e^{-\theta s}\right] \varphi(s)\, ds.$$

Proof. The result follows by applying Fubini's Theorem to $H_t^J = \int_0^t P_s^J \varphi(s)\, ds$ and substituting the explicit expression for the first moment of P_s^J.

2.2. Model II: A non-negative rate via the CIR process

As an alternative to the previous framework, we consider modeling $(P_t^C : t \geq 0)$ as a CIR process. The use of CIR-type dynamics is motivated by their ability to capture mean-reverting stochastic behaviors while preserving positivity, a feature that has made them widely used in applied probability and

in the modeling of time-varying rates. In the context of epidemic modeling, such processes provide a natural way to represent transmission intensities that fluctuate around a typical level while allowing occasional large excursions. Unlike the Jacobi process, the CIR process does not possess an upper bound. The resulting joint dynamics are governed by the following system:

$$\begin{cases} dS_t = -P_t^C \varphi(t) S_t (1 - S_t)\, dt, \\ dP_t^C = \kappa(\eta - P_t^C)\, dt + \sigma \sqrt{P_t^C}\, dW_t, \end{cases} \tag{2.4}$$

where κ, η, and σ are positive constants.

To ensure strict positivity and the existence of a unique stationary distribution, we assume that the parameters satisfy the following Feller condition:

$$2\kappa\eta > \sigma^2.$$

Under this condition, the process remains strictly positive almost surely and admits a stationary Gamma distribution with a shape parameter $2\kappa\eta/\sigma^2$ and a scale parameter $\sigma^2/2\kappa$ [16]. Moreover,

$$\mathbb{E}[P_t^C] = \eta + (p_0 - \eta)e^{-\kappa t}, \qquad t \geq 0,$$

which converges to the long-term mean η as $t \to \infty$.

The following lemma provides the analytical form of the expected integrated intensity under the CIR model. This result is used to verify the integrability condition $\mathbb{E}[H_\infty] < \infty$ required in the asymptotic analysis.

Lemma 2.5. *Under the CIR framework, the expected Integrated Transmission Intensity at time $t \geq 0$ is given by the following:*

$$\mathbb{E}[H_t^{CIR}] = \int_0^t \left[\eta + (p_0 - \eta)e^{-\kappa s}\right] \varphi(s)\, ds.$$

A key advantage of the CIR process lies in its affine diffusion structure. By the Feynman–Kac Theorem, this property yields a closed-form expression for the Laplace transform of H_t^{CIR} under the non-intervention regime ($\varphi \equiv 1$).

Proposition 2.6. *Let*

$$H_T^{CIR} = \int_0^T P_s^C\, ds,$$

where $(P_t^C)_{t\geq 0}$ is a CIR process that satisfies

$$dP_t^C = \kappa(\eta - P_t^C)\, dt + \sigma \sqrt{P_t^C}\, dW_t, \qquad P_0^C = p_0.$$

Then, for every $\lambda \geq 0$, the Laplace transform of H_T^{CIR} is given by the following:

$$\mathbb{E}\left[e^{-\lambda H_T^{CIR}} \,\middle|\, P_0^C = p_0\right] = \exp\{-A(T, \lambda) - B(T, \lambda)p_0\},$$

where

$$B(T, \lambda) = \frac{2\lambda\left(e^{\gamma T} - 1\right)}{(\gamma + \kappa)\left(e^{\gamma T} - 1\right) + 2\gamma},$$

and

$$A(T,\lambda) = \frac{2\kappa\eta}{\sigma^2}\ln\left(\frac{2\gamma e^{(\gamma+\kappa)T/2}}{(\gamma+\kappa)(e^{\gamma T}-1)+2\gamma}\right),$$

with

$$\gamma = \sqrt{\kappa^2+2\sigma^2\lambda}.$$

Proof. Let $T > 0$ be fixed. We apply Theorem A.1. Define $u(t,x) = \mathbb{E}_x\left[e^{-\lambda\int_t^T P_s^C\,ds}\right]$. In the notation of Theorem A.1, we choose $f(x) = 1, g(t,x) = 0, k(t,x) = \lambda x$. Observe that $u(T,x) = 1$. Therefore, it suffices to find a function $u \in C^{1,2}([0,T]\times(0,\infty))$ that satisfies the following:

$$\begin{aligned} -\frac{\partial u}{\partial t} + \lambda x u &= Lu, \\ u(T,x) &= 1, \end{aligned} \tag{2.5}$$

where L denotes the infinitesimal generator associated with the following CIR process:

$$L = \kappa(\eta - x)\frac{\partial}{\partial x} + \frac{1}{2}\sigma^2 x\frac{\partial^2}{\partial x^2}.$$

Motivated by the affine structure of the CIR generator, we seek a solution of the following form:

$$u(t,x) = e^{-[A(T-t)+B(T-t)x]},$$

where $A(0) = B(0) = 0$. Notice that this choice guarantees the terminal condition $u(T,x) = 1$.

A direct computation yields

$$\frac{\partial u}{\partial t} = \left(A'(T-t) + B'(T-t)x\right)u,$$

and

$$Lu = -\kappa(\eta - x)B(T-t)u + \frac{1}{2}\sigma^2 x B^2(T-t)u.$$

By substituting into (2.5) and dividing by u, we obtain the following:

$$-A'(T-t) - B'(T-t)x + \lambda x = -\kappa\eta B(T-t) + \kappa x B(T-t) + \frac{1}{2}\sigma^2 x B^2(T-t).$$

By identifying constant and linear terms in x, we deduce the system ($\tau = T - t$)

$$\begin{aligned} A'(\tau) &= \kappa\eta B(\tau), \\ B'(\tau) &= \lambda - \kappa B(\tau) - \frac{1}{2}\sigma^2 B^2(\tau), \end{aligned}$$

with

$$A(0) = 0, \qquad B(0) = 0.$$

The equation satisfied by B is a classical Riccati differential equation. Its explicit solution is the following:

$$B(\tau,\lambda) = \frac{2\lambda(e^{\gamma\tau}-1)}{(\gamma+\kappa)(e^{\gamma\tau}-1)+2\gamma},$$

where

$$\gamma = \sqrt{\kappa^2 + 2\sigma^2\lambda}.$$

By integrating the equation for A, we obtain the following:

$$A(\tau, \lambda) = \frac{2\kappa\eta}{\sigma^2} \ln\left(\frac{2\gamma e^{(\gamma+\kappa)\tau/2}}{(\gamma+\kappa)(e^{\gamma\tau}-1)+2\gamma}\right).$$

Finally, evaluating at $t = 0$, we have the following:

$$u(0, p_0) = \mathbb{E}\left[e^{-\lambda H_T^{CIR}} \,\middle|\, P_0^C = p_0\right];$$

therefore,

$$\mathbb{E}\left[e^{-\lambda H_T^{CIR}} \,\middle|\, P_0^C = p_0\right] = \exp\{-A(T, \lambda) - B(T, \lambda)p_0\}.$$

2.3. Random time to reach infection thresholds in the non-modulated regime

While our primary focus is on asymptotic behavior, the framework also provides insight into finite-time dynamics through the analysis of hitting times and probabilistic bounds. In particular, the use of moment generating functions and Chernoff-type estimates allows us to characterize the probability of reaching critical infection levels within a finite time horizon.

In [7], the authors investigated the time required for the proportion of susceptible individuals to reach a specific threshold from a random initial state. Motivated by this, we study the distribution of the corresponding hitting time. While a closed-form expression remains elusive for the unmitigated CIR model, we establish a rigorous bound for its cumulative distribution function. Let $S_0 = s_0 \in (0, 1)$ be the initial susceptible fraction, and let $x \in (0, s_0)$ be a target threshold. Let $\tau \equiv \tau(s_0, x)$ denote the hitting time, defined as the random time at which $S_\tau = x$.

From (2.2), the event $\{\tau \le t\}$ is equivalent to the integrated intensity H_t^{CIR} that exceeds a critical level:

$$\mathbb{P}(\tau \le t) = \mathbb{P}(H_t^{CIR} \ge M),$$

where $M(s_0, x) = \ln\left[\frac{s_0(1-x)}{x(1-s_0)}\right]$ represents the cumulative infection pressure required to reach the target prevalence. We can bound this probability using Chernoff's inequality as follows:

$$\mathbb{P}(\tau \le t) \le \inf_{\lambda>0} e^{-\lambda M}\mathbb{E}[e^{\lambda H_t^{CIR}}]. \tag{2.6}$$

In the baseline scenario ($\varphi \equiv 1$), the moment-generating function (MGF) of H_t^{CIR} is analytically tractable due to the affine structure of the process, thus allowing for a precise characterization of this hitting time distribution.

A similar argument allows us to characterize the MGF of the integrated intensity. Unlike the Laplace transform, the MGF is only well-defined for values of the parameter where the expectation does not diverge, thus leading to a restricted domain.

Proposition 2.7. *Let H_t^{CIR} be the integrated intensity of a CIR process. For any $\lambda \in (0, \lambda_c)$, where $\lambda_c = \frac{\kappa^2}{2\sigma^2}$, the MGF is given by the following:*

$$\mathbb{E}\left[e^{\lambda H_t^{CIR}} \mid P_0 = p_0\right] = \exp\{A(t, \lambda) + B(t, \lambda)p_0\},$$

where the functions A and B are as defined in Proposition 2.6, thereby substituting λ with $-\lambda$ and setting $\gamma = \sqrt{\kappa^2 - 2\sigma^2\lambda}$.

Proof. The proof follows the same steps as in the Laplace transform case by applying the Feynman–Kac Theorem to the expectation $u(t,x) = \mathbb{E}[e^{\lambda\int_0^t P_s\,ds} \mid P_0 = x]$. The resulting system of Riccati equations:

$$\begin{aligned} B'(t) &= \frac{1}{2}\sigma^2 B^2(t) - \kappa B(t) + \lambda, \quad B(0) = 0, \\ A'(t) &= \kappa\eta B(t), \quad A(0) = 0, \end{aligned}$$

possesses a real solution if and only if the discriminant $\Delta = \kappa^2 - 2\sigma^2\lambda$ is positive. This condition is satisfied for $\lambda < \lambda_c$, thus ensuring that the integral intensity does not explode and the MGF remains finite.

The following corollary is an immediate consequence of (2.6) and Proposition 2.7.

Corollary 2.8. *The probability of reaching the infection threshold before time t is bounded by the following:*

$$\mathbb{P}(\tau \le t) \le \inf_{\lambda\in(0,\lambda_c)} \exp(-\lambda M + A(t,\lambda) + B(t,\lambda)p_0). \tag{2.7}$$

Next, we aim to further explore the inequality obtained in the corollary above. Let $t > 0$ be fixed, and let $f : (0,\lambda_c) \to \mathbb{R}$ be defined by the following:

$$f(\lambda) = \exp(-\lambda M + \Lambda_t(\lambda)) \tag{2.8}$$

where $\Lambda_t(\lambda) = A(t,\lambda) + B(t,\lambda)p_0 = \ln\left(\mathbb{E}_{p_0}\left[e^{\lambda H_t^{CIR}}\right]\right)$. Here, we define $\mathbb{E}_{p_0}[\cdot] = \mathbb{E}[\cdot \mid P_0 = p_0]$ as the expectation conditioned on the initial condition p_0. Then, we have the following proposition.

Proposition 2.9. *Let $t > 0$ be fixed. If $M > \mathbb{E}_{p_0}[H_t^{CIR}]$, then the following hold:*

(i) f is strictly convex on $(0,\lambda_c)$ and reaches its minimum value in $(0,\lambda_c)$.

(ii) Let $\lambda^*(M)$ be the point that minimizes the function $f(\lambda)$ in $(0,\lambda_c)$. Then, $\lambda^*(M)$ is a strictly increasing function of M, and

$$\lim_{M\uparrow\infty} \lambda^*(M) = \lambda_c = \frac{\kappa^2}{2\sigma^2}.$$

Proof. (i) To show the strict convexity of $f(\lambda)$, it is sufficient to analyze the function $G(\lambda) = -\lambda M + \Lambda_t(\lambda)$ for $\lambda \in (0,\lambda_c)$. First, we analyze the differentiability of $\Lambda_t(\lambda)$. Let $\lambda \in (0,\lambda_c)$ be fixed, and let $\epsilon > 0$ be such that $(\lambda-\epsilon,\lambda+\epsilon) \subset (0,\lambda_c)$. For any $h \in (-\epsilon,\epsilon)$ and $k \in \mathbb{N}$, note that $x^k e^{(\lambda+h)x} \le Ce^{(\lambda+\epsilon)x}$ for all $x > 0$, where C is a constant depending on k. This allows the application of the Dominated Convergence Theorem to obtain the following:

$$\Lambda_t'(\lambda) = \frac{\mathbb{E}_{p_0}[H_t^{CIR}e^{\lambda H_t^{CIR}}]}{\mathbb{E}_{p_0}[e^{\lambda H_t^{CIR}}]},$$

and

$$\Lambda_t''(\lambda) = \frac{\mathbb{E}_{p_0}[e^{\lambda H_t^{CIR}}]\mathbb{E}_{p_0}[(H_t^{CIR})^2 e^{\lambda H_t^{CIR}}] - (\mathbb{E}_{p_0}[H_t^{CIR}e^{\lambda H_t^{CIR}}])^2}{(\mathbb{E}_{p_0}[e^{\lambda H_t^{CIR}}])^2}.$$

By applying the Esscher transform, which is defined as:

$$\mathbb{P}_\lambda(d\omega) = \frac{e^{\lambda H_t^{CIR}(\omega)}}{\mathbb{E}_{p_0}[e^{\lambda H_t^{CIR}}]}\mathbb{P}(d\omega),$$

we observe that $\Lambda_t'(\lambda) = \mathbb{E}_{\mathbb{P}_\lambda}[H_t^{CIR}]$ and $\Lambda_t''(\lambda) = \mathrm{Var}_{\mathbb{P}_\lambda}(H_t^{CIR}) > 0$, since $\sigma > 0$ implies that H_t^{CIR} is a non-degenerate random variable.

Given that $G''(\lambda) = \Lambda_t''(\lambda) > 0$, it follows that:

$$f''(\lambda) = e^{G(\lambda)}[G''(\lambda) + (G'(\lambda))^2] > 0.$$

Thus, f is strictly convex. To prove the existence of a unique minimum in the interior of the interval, we examine the boundary behavior of $G'(\lambda) = \Lambda_t'(\lambda) - M$:

- Using the Dominated Convergence Theorem again, $\lim_{\lambda\downarrow 0}\Lambda_t'(\lambda) = \mathbb{E}_{p_0}[H_t^{CIR}]$. Since $M > \mathbb{E}_{p_0}[H_t^{CIR}]$, it follows that $\lim_{\lambda\downarrow 0} G'(\lambda) < 0$.
- Note that $A(t,\lambda)$ and $B(t,\lambda)$ converge to ∞ as $\lambda \uparrow \lambda_c$; therefore, $\lim_{\lambda\uparrow\lambda_c}\Lambda_t'(\lambda) = \infty$, which implies $\lim_{\lambda\uparrow\lambda_c} G'(\lambda) > 0$.

By the Intermediate Value Theorem, there exists a unique $\lambda^*(M) \in (0,\lambda_c)$ such that $G'(\lambda^*) = 0$, thus confirming that f reaches a global minimum.

(ii) The optimal point $\lambda^*(M)$ is implicitly defined by the condition $\Lambda_t'(\lambda^*) = M$. By applying the Implicit Function Theorem, we obtain the following:

$$\frac{d\lambda^*}{dM} = \frac{1}{\Lambda_t''(\lambda^*)} = \frac{1}{\mathrm{Var}_{\mathbb{P}_{\lambda^*}}(H_t^{CIR})} > 0.$$

This shows that $\lambda^*(M)$ is strictly increasing in M. Furthermore, since $\Lambda_t'(\lambda)$ is a continuous, strictly increasing mapping from $(0,\lambda_c)$ to $(\mathbb{E}_{p_0}[H_t^{CIR}],\infty)$, the condition $M \to \infty$ forces $\lambda^*(M)$ to approach λ_c to satisfy the equality $\Lambda_t'(\lambda^*) = M$.

3. Numerical studies

For the numerical simulation of the CIR process, we use a truncated Euler–Maruyama scheme. In particular, the diffusion term is evaluated as $\sqrt{\max(P_t,0)}$, which prevents numerical instabilities when the discretized process takes small negative values. All simulations are performed with sufficiently small time steps to ensure numerical stability.

3.1. The Jacobi case: Simulations and discussion

To assess the practical dynamics of the model, we conduct numerical simulations using the Euler–Maruyama discretization scheme. We generate an ensemble of $N_{\text{sim}} = 50$ trajectories over a time horizon $T = 15.0$ with a time step of $\Delta t = 5 \times 10^{-3}$. For these simulations, the parameter set is fixed at $(\theta,\mu,\sigma) = (2.0, 0.4, 0.3)$ and the upper bound is set to $a = 1.0$, with initial conditions $p_0 = 0.5$ and $S_0 = 0.99$.

3.1.1. Baseline scenario: Non-modulated regime

($\varphi \equiv 1$). In this case, we examine the system under the non-modulated regime. As illustrated in Figure 1, the transmission intensity P_t^J exhibits stochastic fluctuations confined to the interval $(0, a)$. Consistent with Theorem 2.3, the integrated intensity H_t grows linearly as $t \to \infty$. Consequently, the infected fraction $1 - S_t$ converges to unity along the simulated trajectories.

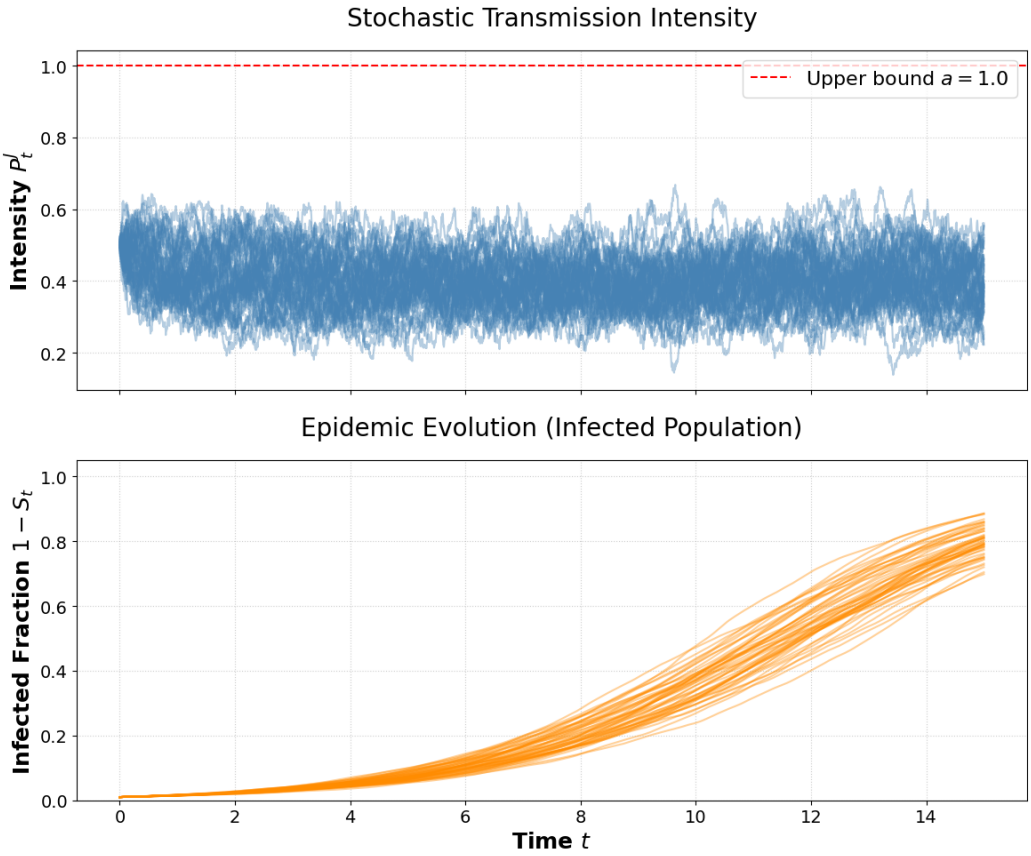

Figure 1. Stochastic trajectories of the Jacobi transmission intensity P_t^J (top) and the corresponding infected fraction $1 - S_t$ (bottom) for the baseline case $\varphi \equiv 1$. The trajectories illustrate the inevitable saturation of the epidemic ($1 - S_t \to 1$) as the cumulative intensity H_t diverges.

3.1.2. Scenario with exponential modulation

Now, we analyze the exponentially modulated regime defined by $\varphi(t) = e^{-0.2t}$. In this case, the effective transmission rate $\beta_t = \varphi(t)P_t^J$ decreases over time due to the decay of the modulation function. Figure 2 illustrates the behavior predicted by Theorem 2.2. Although the stochastic process P_t^J remains active, the decay of $\varphi(t)$ ensures that the integrated intensity H_t converges almost surely to a finite random variable H_∞. Consequently, the infected fraction does not converge to unity, and a positive susceptible fraction remains in the long-term regime, as shown in the bottom panel.

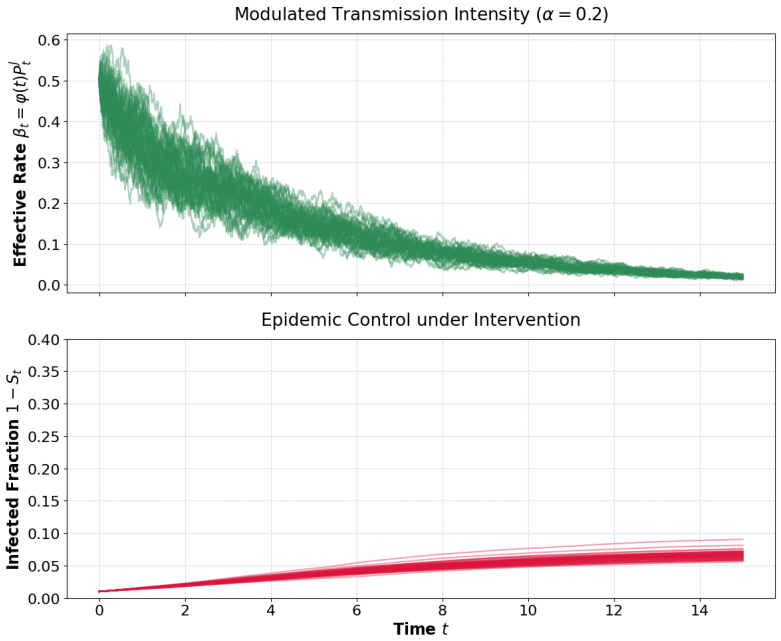

Figure 2. System dynamics under exponential modulation $\varphi(t) = e^{-0.2t}$. The top panel shows the effective transmission rate $\beta_t = \varphi(t)P_t^J$ decaying towards zero, while the bottom panel illustrates that the infected fraction $1 - S_t$ stabilizes below one, leaving a positive susceptible fraction in the long-term regime.

3.2. The CIR case: Simulations and discussion

Numerical simulations for the CIR framework were performed using the same discretization settings ($T = 15$, $\Delta t = 5 \times 10^{-3}$) and initial conditions ($p_0 = 0.5$, $S_0 = 0.99$) as in the Jacobi case. We generated $N_{\text{sim}} = 50$ independent trajectories. The structural parameters for the CIR process were set to $(\kappa, \eta, \sigma) = (2.0, 0.4, 0.3)$, thus satisfying the Feller condition ($2\kappa\eta > \sigma^2$) to ensure the transmission rate remains strictly positive.

3.2.1. Baseline scenario: Non-modulated regime

($\varphi \equiv 1$). In the non-modulated regime, the transmission rate is solely driven by the CIR process ($\beta_t = P_t^C$). Under this setting, the integrated intensity H_t diverges almost surely as $t \to \infty$. Consequently, the infected fraction $1 - S_t$ converges to unity along the simulated trajectories, as illustrated in Figure 3.

Numerical simulations were performed using the discretization parameters ($T = 15, \Delta t = 5 \times 10^{-3}$) and initial conditions ($p_0 = 0.5, S_0 = 0.99$). The parameters for the CIR process were set to $(\kappa, \eta, \sigma) = (2, 0.4, 0.3)$ and we used $N_{\text{sim}} = 50$ trajectories.

3.2.2. Scenario with exponential modulation

Now, we consider simulations with the exponential intervention $\varphi(t) = e^{-0.2t}$. As Figure 4 illustrates, the transmission rate $\beta_t = \varphi(t)P_t^C$ decays sufficiently fast to ensure that the integrated intensity process H_t remains a.s. finite. This creates a "continuous curbing effect", thereby preventing the eventual infection of the entire population.

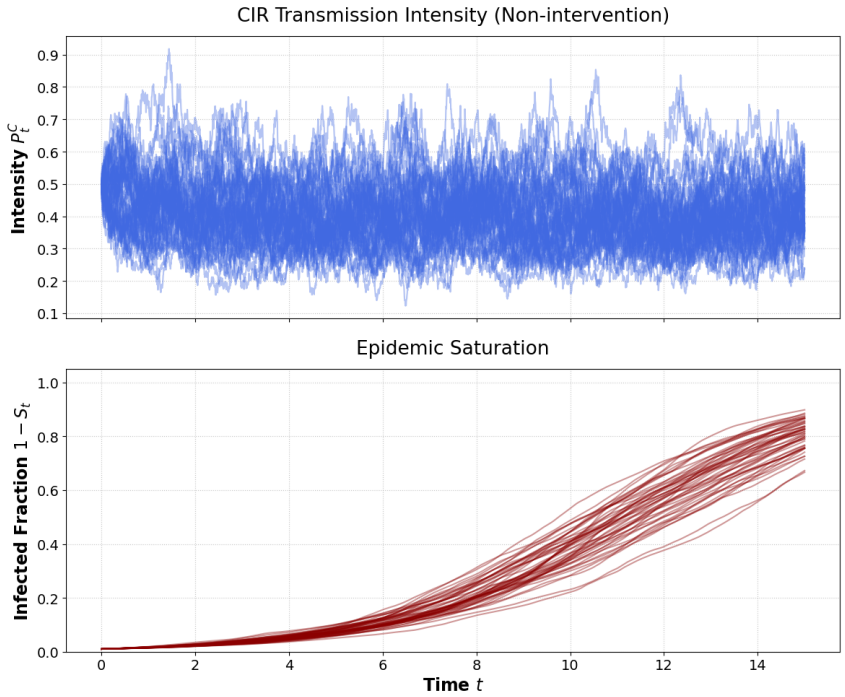

Figure 3. Temporal evolution of the CIR transmission rate P_t^C (top) and the resulting infected fraction $1 - S_t$ (bottom) for $\varphi \equiv 1$. As t increases, the cumulative intensity H_t drives the infected fraction towards unity.

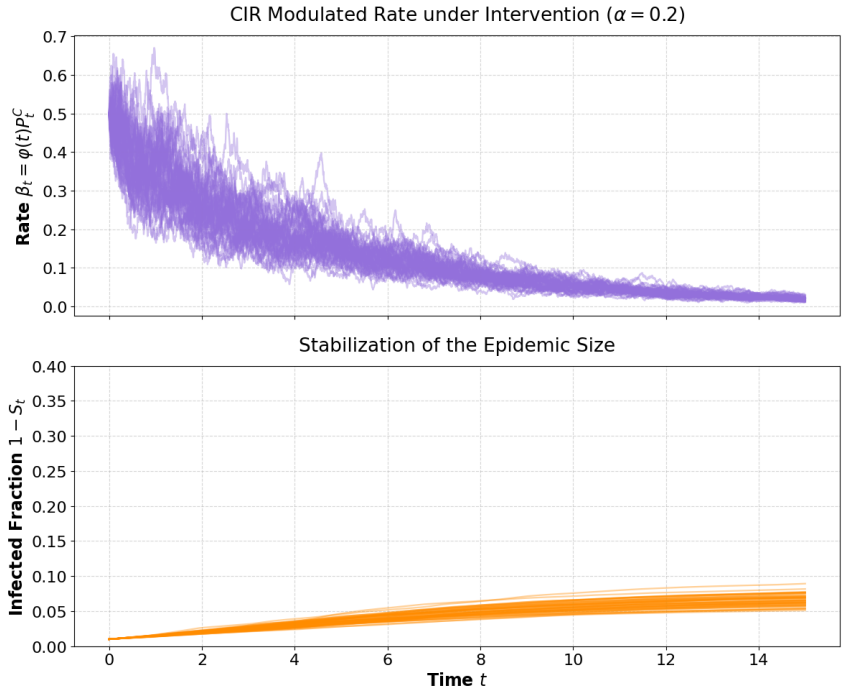

Figure 4. Epidemic dynamics under exponential modulation $\varphi(t) = e^{-0.2t}$. The top panel displays the effective transmission rate, while the bottom panel shows the corresponding evolution of the infected fraction.

Remark. The integrated intensity $(H_t^{CIR}; t \geq 0)$ under the CIR process is analytically tractable in the non-modulated regime. In particular, the affine structure of the process yields a closed-form expression for the Laplace transform of H_t^{CIR}, which allows the explicit computation of its moments.

3.3. Simulation of threshold times without intervention under the CIR process

To numerically illustrate the random time to reach infection thresholds in the non-modulated CIR regime, we set the model parameters to $\kappa = 2$, $\eta = 0.4$, $p_0 = 0.5$, and $t = 1$. Under these settings, the expected integrated intensity is $\mathbb{E}_{p_0}[H_1^{CIR}] \approx 0.443$. To study the dependence of the optimal parameter and the corresponding probability bounds, we consider thresholds $M \in \{0.3, 0.5, 0.55, 0.6, 0.65, 0.7\}$.

As illustrated in Figure 5, when $M = 0.3$, the bound is trivial, since it equals 1. For values of M above the mean, the optimizer $\lambda^*(M)$ approaches the singularity λ_c. At the same time, the minimum value of $f(\lambda)$ decreases as M increases. For example, the probability bound is approximately 0.88 when $M = 0.5$, while for $M = 0.7$, it decreases to approximately 0.45.

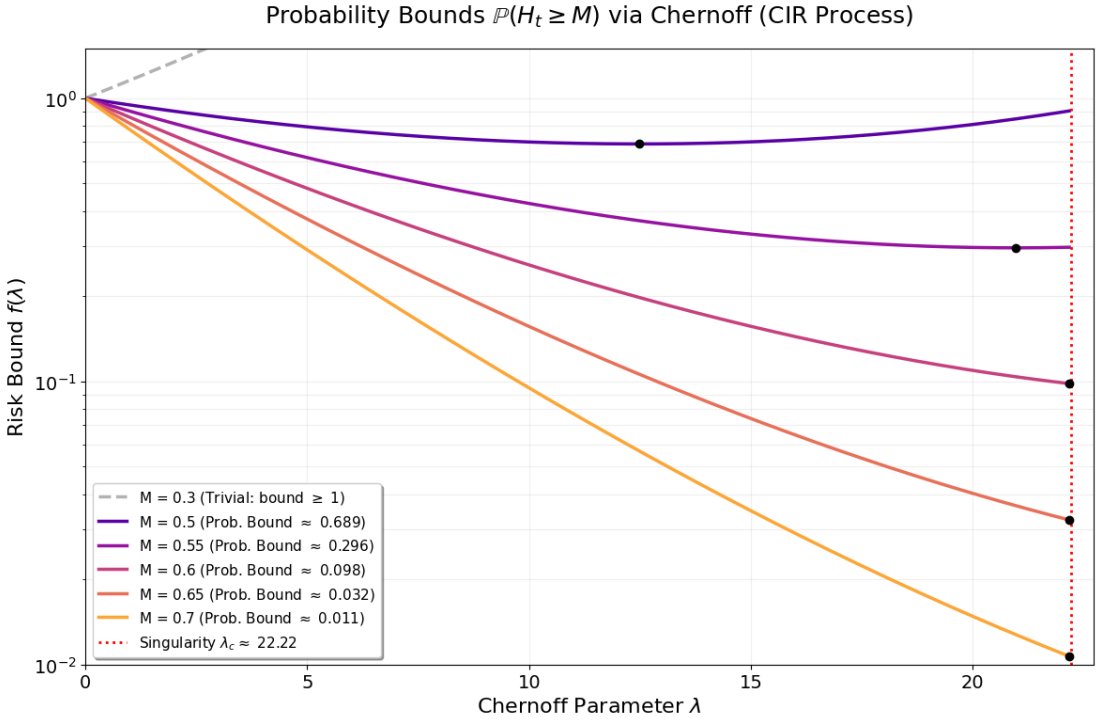

Figure 5. Sensitivity of the risk bound $f(\lambda)$ and corresponding probability bounds across different regimes of M. The legend displays the approximate value of the tightest Chernoff bound $f(\lambda^*)$, which acts as an upper bound for the probability of reaching the infection threshold before time $t = 1$.

Beyond matching the first two moments, the key structural difference between the CIR and Jacobi processes lies in their support. The CIR process is unbounded and therefore allows for rare but significant excursions, while the Jacobi process is confined to a bounded interval, thus preventing such extreme deviations. This distinction plays a central role in the observed differences in tail behavior and risk assessment.

4. Numerical comparison of the Jacobi and CIR processes for P_t

4.1. Experimental setup and calibration

The core of our methodology relies on isolating the effect of the process support. Specifically, we aim to contrast the dynamics of the bounded Jacobi process, P_t^J, with those of the unbounded CIR process, P_t^C, thus ensuring that no other statistical factors bias the comparison. To achieve this, we calibrate both models to share the same first two stationary moments, thus allowing us to observe how the difference in their supports affects the epidemic's progression.

First, we align the drift components by setting an identical mean-reversion speed ($\theta_J = \kappa = 0.5$) and a shared long-term average ($\mu = \eta = 0.3$) for both models. For the Jacobi process, we fixed an upper bound of $a = 0.5$ to represent a physical or biological limit on the transmission intensity.

The main challenge in this setup lies in the calibration of the diffusion coefficients. Given that the Jacobi process is physically constrained by its boundaries, its stationary variance is defined by the following expression:

$$\mathrm{Var}[P_\infty^J] = \frac{\sigma_J^2 \mu(a-\mu)}{2\theta_J + a\sigma_J^2}. \tag{4.1}$$

Our procedure consists of selecting a value for σ_J, calculating the resulting variance, and then solving for the specific σ_{CIR} that yields the exact same level of dispersion in the CIR process (where $\mathrm{Var}[P_\infty^C] = \sigma_{CIR}^2 \eta/(2\kappa)$). This ensures that we are strictly controlling for the amount of noise in the system. Consequently, any discrepancy observed in the epidemic dynamics can solely be attributed to the boundary effects rather than differences in the first two moments. To guarantee the robustness of these findings, particularly for rare tail events, we initialize the simulation at $s_0 = 0.99$ and execute $N = 100,000$ Monte Carlo paths.

4.2. Scenario 1: Dynamics in the non-modulated regime ($\varphi \equiv 1$)

In the absence of intervention, both processes eventually lead to the infection of the entire population ($S_t \to 0$ as $t \to \infty$). The objective is to identify how the stochastic drivers differ before this terminal state is reached.

4.2.1. Low volatility regime

By setting $\sigma_J = 0.2$, we obtain a corresponding $\sigma_{CIR} \approx 0.089$ via the moment-matching calibration. We observe the system at a time horizon of $T = 15$. As displayed in Figure 6, the resulting probability density functions for both models are virtually identical. In this low-volatility regime, the process rarely reaches the upper bound $a = 0.5$; consequently, the Jacobi process behaves like an unbounded process near its mean, thus making the structural difference between the two models negligible.

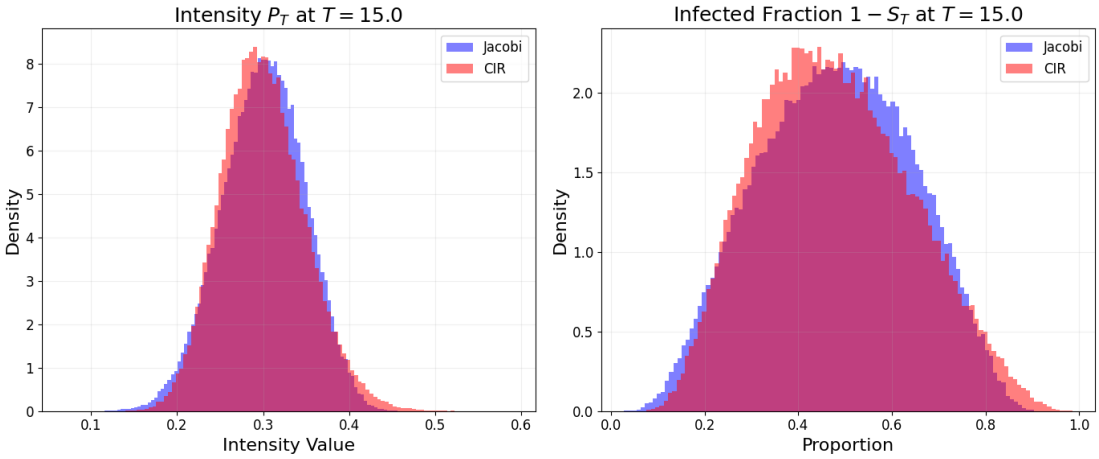

Figure 6. Comparison under Low Volatility ($\sigma_J = 0.2, \sigma_{CIR} \approx 0.089$). The left panel shows the infection intensity P_T, and the right panel shows the epidemic size $1 - S_T$. The distributions overlap almost perfectly, thus demonstrating model equivalence when fluctuations remain far from the boundaries.

4.2.2. High volatility and cumulative pressure ($T = 100$)

By setting the volatility to $\sigma_J = 1.5$ (with a corresponding $\sigma_{CIR} \approx 0.387$) over an extended horizon of $T = 100$, we observe that the final epidemic size, $1 - S_T$, saturates at 1.0 for both models. However, the cumulative transmission intensity, $H_T = \int_0^T \beta_s \, ds$, highlights the fundamental differences between the two frameworks, as illustrated in Figure 7. The CIR process exhibits a heavy right tail because it admits extreme transmission intensities that are structurally non-realizable within the bounded Jacobi framework. This suggests that this tail behavior, rather than the mean dynamics, governs the elevated risk bounds in unbounded models. A similar heavy-tailed behavior has been recently observed in mean-field epidemic models derived from individual-based dynamics, where the asymptotic distribution of epidemic observables may exhibit an inverse-gamma type behavior [17]. This provides additional support for the idea that unbounded stochastic transmission mechanisms, such as the CIR process, can capture extreme outbreak scenarios that are not accessible under bounded dynamics.

4.2.3. Early stage divergence ($T = 10$)

When observing the process up to $t = 10$, the disparity in the behavior of H_t becomes apparent in the fraction of infected individuals. Given that the CIR process is unbounded, it admits significantly larger excursions than the Jacobi process, thereby accelerating the infection dynamics in extreme cases. As displayed in Figure 8, the CIR process generates a heavier right tail in the distribution of the fraction of the population infected ($1 - S_T$) during the early stages of the epidemic. This confirms that even if the stationary means are identical, the lack of a structural ceiling in the CIR framework allows for more rapid outbreaks.

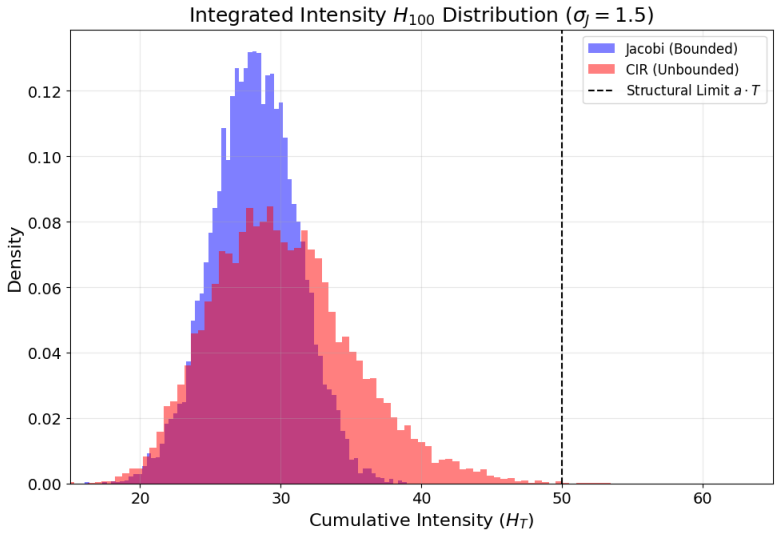

Figure 7. Comparison of the cumulative transmission intensity H_T at $T = 100$. While the epidemic size has saturated, the CIR model (red) assigns significant weight to extreme cumulative intensities that lie far beyond the structural limits of the Jacobi model (blue).

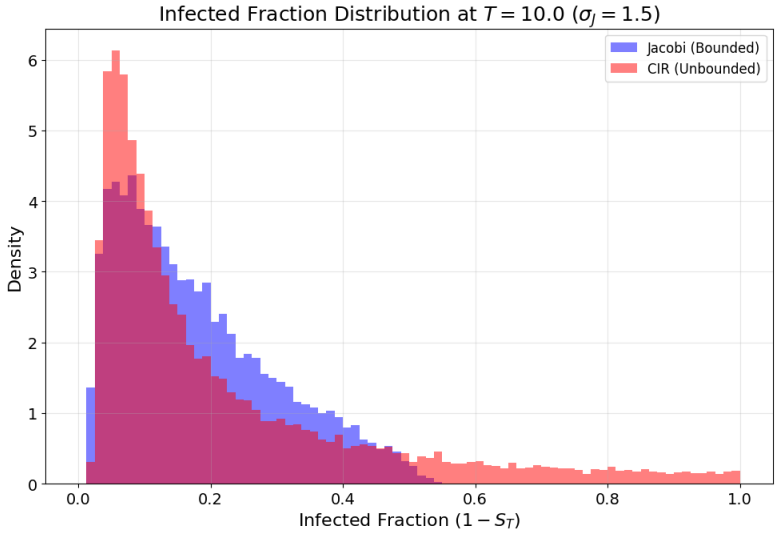

Figure 8. Distribution of the infected fraction $1 - S_T$ at the early stage $T = 10$ under high volatility ($\sigma_J = 1.5, \sigma_{CIR} \approx 0.387$). The comparison shows that the CIR model (red) produces a heavier right tail, thus indicating a higher probability of rapid infection spread compared to the bounded Jacobi model (blue).

4.3. Scenario 2: Exponentially modulated dynamics ($\varphi(s) = e^{-\alpha s}$).

Next, we evaluate the models under the exponentially modulated regime $\varphi(s) = e^{-0.2s}$.

4.3.1. Tail risk and model comparison

In the high-volatility regime ($\sigma_J = 1.5$), the differences between the two models become clearer. Figure 9 illustrates the final epidemic size, $1 - S_\infty$, under exponential modulation. This difference is mainly driven by the heavier right tail observed in the CIR framework. As summarized in Table 1, the upper quantiles significantly differ between the two models: the 95th percentile for the Jacobi model is approximately 0.320, whereas it reaches 0.530 for the CIR model. Although both models are calibrated to share the same stationary mean and variance, the unbounded support of the CIR process leads to larger upper-tail values in high-volatility regimes.

Table 1. Comparison of risk metrics for the final epidemic size ($1 - S_\infty$) under intervention $\varphi(s) = e^{-0.2s}$.

Metric	Jacobi (Bounded)	CIR (Unbounded)
Mean epidemic size	0.185	0.192
95th percentile (VaR)	**0.320**	**0.530**
Maximum observed size	0.460	0.985

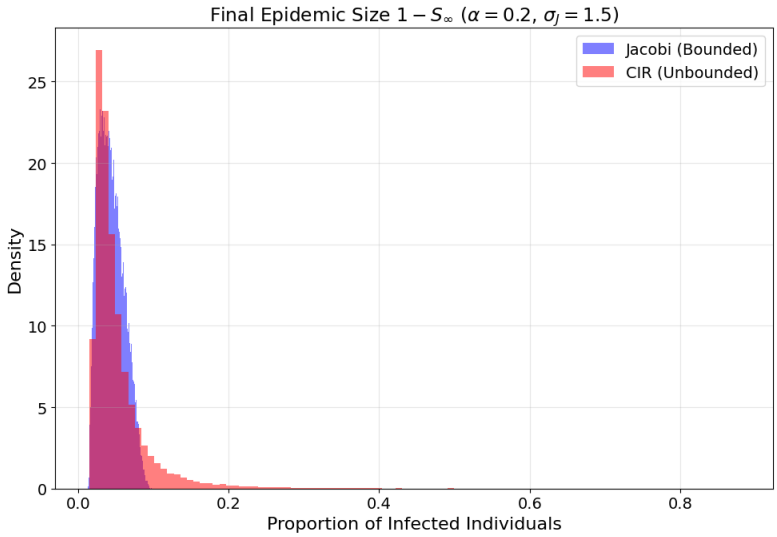

Figure 9. Final epidemic size under exponential modulation $\varphi(s) = e^{-0.2s}$. The bounded support of the Jacobi process (blue) limits the upper tail of the epidemic distribution, whereas the CIR model (red) produces larger upper-tail values under the same modulation regime.

4.3.2. Interpretation of tail divergence

These results are consistent with the theoretical properties of the chosen models. As expected, the unbounded nature of the CIR process allows for higher excursions in the transmission rates compared to the Jacobi model, which is strictly constrained by its upper bound a. Even when both processes are calibrated to the same stationary moments, the lack of a ceiling in the CIR framework naturally leads to a heavier right tail in the distribution of the final epidemic size.

5. Discussion and conclusions

In this work, we compared the Jacobi and CIR processes as stochastic drivers for epidemic dynamics under modulation. Our analysis primarily focused on the CIR framework due to its analytical tractability and its heavier tail behavior. We showed that even when both models are calibrated to share the same stationary mean and variance, the choice of support (bounded versus unbounded) produces substantially different upper-tail behaviors, particularly in high-volatility regimes.

From a modeling perspective, the parameters of the stochastic transmission process admit a natural interpretation. The mean-reversion level determines a typical transmission intensity around which the system fluctuates, while the volatility parameter controls the magnitude of the stochastic fluctuations. Higher volatility increases the probability of large deviations from the average behavior and leads to heavier tails in the epidemic distribution.

Moreover, the proposed framework provides explicit analytical characterizations for quantities associated with transmission variability. In particular, the affine structure of the CIR process yields closed-form expressions for Laplace transforms and Chernoff-type probability bounds associated with the integrated transmission intensity. These bounds provide a tractable way to estimate threshold probabilities in the non-modulated regime.

Additionally, the deterministic modulation function $\varphi(t)$ plays an important role in the asymptotic behavior of the model. In particular, integrable modulation functions alter the long-term regime by keeping the cumulative transmission intensity finite. In this sense, the framework may also provide a basis to estimate $\varphi(t)$ from the transmission data observed before and after changes in the epidemic dynamics.

Several mathematical and statistical questions remain open for future work. These include the estimation of model parameters from epidemic data, the study of inference problems associated with each stochastic framework, and the derivation of explicit formulas for broader classes of modulation functions.

Extensions that involve empirical calibration, hybrid epidemic frameworks, or heterogeneous population structures remain outside the scope of the present work, but constitute natural directions for future research.

Computational reproducibility

The source code used for the numerical simulations and figures presented in this work is publicly available at the following GitHub repository: https://github.com/duvancatan/Modeling_CIR.

The repository contains implementations of the Jacobi and CIR stochastic processes, the Euler–Maruyama discretization schemes, and the scripts used to reproduce the numerical experiments and graphical results presented in the manuscript.

Use of AI tools declaration

The authors declare they have not used Artificial Intelligence (AI) tools in the creation of this article.

Conflict of interest

The authors declare there is no conflict of interest.

References

1. W. H. Hamer, The Milroy lectures on epidemic disease in England: the evidence of variability and of persistency of type, *Lancet*, **167** (1906), 733–739. https://doi.org/10.1016/S0140-6736(01)80340-8
2. R. Ross, *The Prevention of Malaria*, John Murray, London, 1911.
3. W. O. Kermack, A. G. McKendrick, A contribution to the mathematical theory of epidemics, *Proc. R. Soc. London, Ser. A*, **115** (1927), 700–721. https://doi.org/10.1098/rspa.1927.0118
4. J. D. Murray, *Mathematical Biology I: An Introduction*, Springer, New York, 2002. https://doi.org/10.1007/b98868
5. H. W. Hethcote, The mathematics of infectious diseases, *SIAM Rev.*, **42** (2000), 599–653. https://doi.org/10.1137/S0036144500371907
6. F. Brauer, C. Castillo-Chavez, *Mathematical Models in Population Biology and Epidemiology*, Springer, New York, 2012. https://doi.org/10.1007/978-1-4614-1686-9
7. B. Kegan, R. W. West, Modeling the simple epidemic with deterministic differential equations and random initial conditions, *Math. Biosci.*, **195** (2005), 179–193. https://doi.org/10.1016/j.mbs.2005.02.004
8. W. Wang, Y. Cai, Z. Ding, Z. Gui, A stochastic differential equation SIS epidemic model incorporating Ornstein–Uhlenbeck process, *Physica A*, **509** (2018), 921–936. https://doi.org/10.1016/j.physa.2018.06.099
9. V. V. L. Albani, J. P. Zubelli, Stochastic transmission in epidemiological models, *J. Math. Biol.*, **88** (2024), 25. https://doi.org/10.1007/s00285-023-02042-z
10. S. Hussain, N. Iqbal, E. N. Madi, M. Bakouri, I. Khan, W. S. Koh, On the stochastic modeling and forecasting of the SVIR epidemic dynamic model under environmental white noise, *AIMS Math.*, **10** (2025), 3983–3999. https://doi.org/10.3934/math.2025186
11. J. Guerrero, M. C. Galiano, G. Orlando, Modeling COVID-19 pandemic with financial markets models: The case of Jaén (Spain), *Math. Biosci. Eng.*, **20** (2023), 9080–9100. https://doi.org/10.3934/mbe.2023399
12. G. Orlando, M. Bufalo, V. Nazarova, Modeling COVID-19 response in Cuba: a hybrid approach combining agent-based modeling and time series analysis, *Popul. Health Metrics*, **23** (2025), 71. https://doi.org/10.1186/s12963-025-00382-0
13. G. Orlando, Multi-dimensional scaling of healthcare system profiles and pandemic outcomes in Cuba, Spain, Italy, and Germany, *Health Policy Technol.*, **15** (2026), 101120. https://doi.org/10.1016/j.hlpt.2025.101120
14. R. Khasminskii, *Stochastic Stability of Differential Equations*, Springer, Heidelberg, 2012. https://doi.org/10.1007/978-3-642-23280-0

15. F. Delbaen, H. Shirakawa, An interest rate model with upper and lower bounds, *Asia-Pac. Financ. Mark.*, **9** (2002), 191–209. https://doi.org/10.1023/A:1024125430287

16. J. C. Cox, J. E. Ingersoll, S. A. Ross, A theory of the term structure of interest rates, *Econometrica*, **53** (1985), 385–407. https://doi.org/10.2307/1911242

17. G. Martalò, G. Toscani, M. Zanella, Individual-based foundation of SIR-type epidemic models: mean-field limit and large-time behaviour, *Proc. R. Soc. A*, **481** (2025), 20250633. https://doi.org/10.1098/rspa.2025.0633

18. I. Karatzas, S. E. Shreve, *Brownian Motion and Stochastic Calculus*, Springer, New York, 1991. https://doi.org/10.1007/978-1-4612-0949-2

19. A. Alfonsi, *Affine Diffusions and Related Processes: Simulation, Theory and Applications*, Springer, Cham, 2015. https://doi.org/10.1007/978-3-319-05221-2

20. D. Duffie, D. Filipović, W. Schachermayer, Affine processes and applications in finance, *Ann. Appl. Probab.*, **13** (2003), 984–1053. https://doi.org/10.1214/aoap/1060202833

21. M. J. Keeling, P. Rohani, *Modeling Infectious Diseases in Humans and Animals*, Princeton University Press, Princeton, 2008.

22. F. C. Klebaner, *Introduction to Stochastic Calculus with Applications*, Imperial College Press, London, 2005.

23. B. Øksendal, *Stochastic Differential Equations: An Introduction with Applications*, Springer, Berlin, 2003. https://doi.org/10.1007/978-3-642-14394-6

24. S. E. Shreve, *Stochastic Calculus for Finance II: Continuous-Time Models*, Springer, New York, 2004. https://doi.org/10.1007/978-0-387-22527-2

25. P. F. Verhulst, Notice sur la loi que la population suit dans son accroissement, *Corresp. Math. Phys.*, **10** (1838), 113–129.

Appendix

A. Feynman–Kac representation for the CIR functional

In this appendix, we justify the use of the Feynman–Kac representation for the exponential functionals associated with the CIR process considered in Proposition 2.6. The following version of the Feynman–Kac theorem is adapted from Theorem 7.6, p. 366, in [18]. We include it here for completeness, since the CIR diffusion considered in Proposition 2.6 does not satisfy global Lipschitz conditions at the origin.

Assume that the following stochastic differential equation admits a unique solution as follows:

$$X_t^x = x + \int_0^t b(X_s)\,ds + \int_0^t \sigma(X_s)\,dW_s, \qquad t \geq 0. \tag{A.1}$$

Moreover, assume that the coefficients b and σ are continuous and satisfy the linear growth condition

$$\|b(x)\| + \|\sigma(x)\| \leq C(1 + \|x\|),$$

for some constant $C > 0$. Let $T > 0$ be arbitrary but fixed. Let $f : \mathbb{R}^d \to \mathbb{R}$, $g, k : [0, T] \times \mathbb{R}^d \to \mathbb{R}$ be continuous functions which satisfy the following:

1) $|f(x)| \leq C(1 + \|x\|^{2\lambda})$, $\quad \forall x \in \mathbb{R}^d$,
2) $|g(t, x)| \leq C(1 + \|x\|^{2\lambda})$, $\quad \forall (t, x) \in [0, T] \times \mathbb{R}^d$,

for some constants $C > 0$ and $\lambda \geq 1$. Let L denote the infinitesimal generator associated with (A.1).

Theorem A.1. *Suppose that $u : [0, T] \times \mathbb{R}^d \to \mathbb{R}$ belongs to the class $C^{1,2}([0, T] \times \mathbb{R}^d)$ and satisfies the Cauchy problem*

$$-\frac{\partial u}{\partial t} + ku = Lu + g, \qquad \text{in } [0, T] \times \mathbb{R}^d, \tag{A.2}$$

with the terminal condition

$$u(T, x) = f(x), \qquad x \in \mathbb{R}^d. \tag{A.3}$$

Furthermore, assume that

$$\max_{0 \leq t \leq T} |u(t, x)| \leq M(1 + \|x\|^{2\mu}), \qquad x \in \mathbb{R}^d, \tag{A.4}$$

for some constants $M > 0$ and $\mu \geq 1$. Then, $u(t, x)$ admits the following stochastic representation:

$$u(t, x) = \mathbb{E}_x\left[f(X_T) \exp\left(-\int_t^T k(s, X_s)\, ds \right) + \int_t^T g(r, X_r) \exp\left(-\int_t^r k(\ell, X_\ell)\, d\ell \right) dr \right], \tag{A.5}$$

for all $(t, x) \in [0, T] \times \mathbb{R}^d$. In particular, such a solution is unique.

Remark. Although the theorem is stated for functions defined on the whole space $\mathbb{R}^d$, this is not essential for our application. In the CIR framework, the process $(P_t)_{t \geq 0}$ remains non-negative almost surely. Therefore, it is sufficient that the drift, diffusion coefficient, and the functions involved in the Feynman–Kac representation be defined on $(0, \infty)$, since all compositions with the stochastic process are only evaluated on this domain.

AIMS Press